



# Thin-film electrode based on zeolitic imidazolate frameworks (ZIF-8 and ZIF-67) with ultra-stable performance as a lithium-ion battery anode

Zhen Li<sup>1</sup>, Xiaoxiong Huang<sup>1</sup>, Chuanling Sun<sup>1</sup>, Xiangyu Chen<sup>1</sup>, Jinbo Hu<sup>2</sup>, Andreas Stein<sup>2</sup>, and Bohejin Tang<sup>1,\*</sup>

<sup>1</sup>College of Chemistry and Chemical Engineering, Shanghai University of Engineering Science, Shanghai 201620, People's Republic of China

<sup>2</sup>Department of Chemistry, University of Minnesota, 207 Pleasant St. SE, Minneapolis, MN 55455, USA

Received: 16 August 2016

Accepted: 7 December 2016

Published online:

19 December 2016

© Springer Science+Business Media New York 2016

## ABSTRACT

Thin-film electrodes were prepared using a one-step drop-casting strategy without polymer binder and carbon black. The electrodes exhibit a thin-layer structure, which is an intriguing architecture for lithium-ion battery applications. A high reversible capacity (335.3 and 311.6 mAh g<sup>-1</sup> for ZIF-8 and ZIF-67, respectively), good rate performance, and exceptionally cycling stability (about 95.5% initial capacity was retained after 100 cycles at a high current rate of 5 C) were observed in this study. Such an excellent electrochemical performance of the film electrodes is attributed to the thin-layer architecture, which provides easy access for Li<sup>+</sup> ions to permeate the whole electrodes because of the shortened diffusion paths, and also to the unique property of the MOFs without the collapse of its structure.

## Introduction

Along with the growing demand for high-performance lithium-ion batteries (LIBs), there is a need for the development of novel anode materials to improve the capacity, cycle life, and rate performance of LIBs [1]. Some metals that can reversibly form alloys with lithium are promising alternative anode materials for LIBs because of their high theoretical capacities, such as silicon (forming the SiLi<sub>4.4</sub> alloy, 4200 mAh g<sup>-1</sup>), tin (forming the SnLi<sub>4.4</sub> alloy, 993 mAh g<sup>-1</sup>), antimony (forming the SbLi<sub>3</sub> alloy, 660 mAh g<sup>-1</sup>),

aluminum (forming the LiAl alloy, 994 mAh g<sup>-1</sup>), and germanium (forming the Li<sub>22</sub>Ge<sub>5</sub> alloy, 1600 mAh g<sup>-1</sup>) [2, 3]. However, these metals undergo very large volume changes during the alloying and dealloying processes, resulting in fast capacity degradation. As a novel class of porous materials, metal-organic frameworks (MOFs) have attracted much attention for energy storage and conversion applications such as LIBs [4], fuel cells [5], and supercapacitors [6] due to their porous architecture that allows rapid insertion of species and offers improved electrochemical properties [4], [7]. More importantly,

Address correspondence to E-mail: tangbohejin@sues.edu.cn

MOFs have the ability to deliver a high capacity with good rate performance, such as the Mn-BTC MOF with the theoretical capacity of 833 mAh g<sup>-1</sup> [4]. Therefore, various MOFs with different organic ligands and central metal ions have been investigated as anode materials for LIBs, such as Ni-MOFs [8], Fe-MOF [9], Co-MOF [10], and Zn-imidazole MOF [11]. However, the poor electrical conductivity of MOFs limited their practical application for energy storage and conversion, and the purposeful preparation of highly electrically conductive MOFs is still a big challenge [12].

Recently, many efforts have been made to improve the electrical conductivity of MOFs. Long and co-workers grafted lithium *tert*-butoxide into dehydrated UIO-66, which remarkably improved the ionic conductivity due to the presence of Li<sup>+</sup> ions [13]. Our group has also made some attempts to prepare electrically conductive MOFs by calcining MOFs under nitrogen atmosphere [14]. The guest molecules in MOF pores could become the precursor of carbon, resulting in the improvement of electrochemical activity. These stimulating studies demonstrate the promising future of MOFs as electrode materials. However, in these studies, MOFs have to be mixed with conductive additives and binder to improve electrochemical properties. Few reports have focused on the preparation of MOF thin-film electrodes without conducting additives and binders [15]. Electrodes with thin-film architecture are desirable for electrochemical applications, because avoiding the use of polymer binder can significantly reduce the inactive interface [16]. Also, this thin-film structure can reduce the equivalent series resistance of electrodes and show high power densities [17].

Herein, we report a method of preparing thin-film electrodes by direct drop casting of slurries of zeolitic imidazolate frameworks (ZIFs, a particular class of MOFs) onto a piece of Cu foil current collector. Thin-film electrodes were prepared by this one-step method and the electrochemical performance of these film electrodes as anodes for LIBs was studied. This one-step drop-casting preparation approach has several unique advantages compared to its alternatives, such as thermal oxidation [18], electrochemical deposition [15, 19], and anodic oxidation [20]. The facile preparation route can avoid high-temperature heat treatment and careful control of the reaction conditions suitable for electrochemical deposition [19]. In addition, the quality of the coating obtained

by this strategy in terms of coverage is better than that typically obtained by electrochemical deposition [15]. Also, this thin film is suitable for fundamental studies of the electrochemical performance of MOFs because of the elimination of the effect of conducting additives and binders on electrochemical properties.

## Experimental

### Synthesis

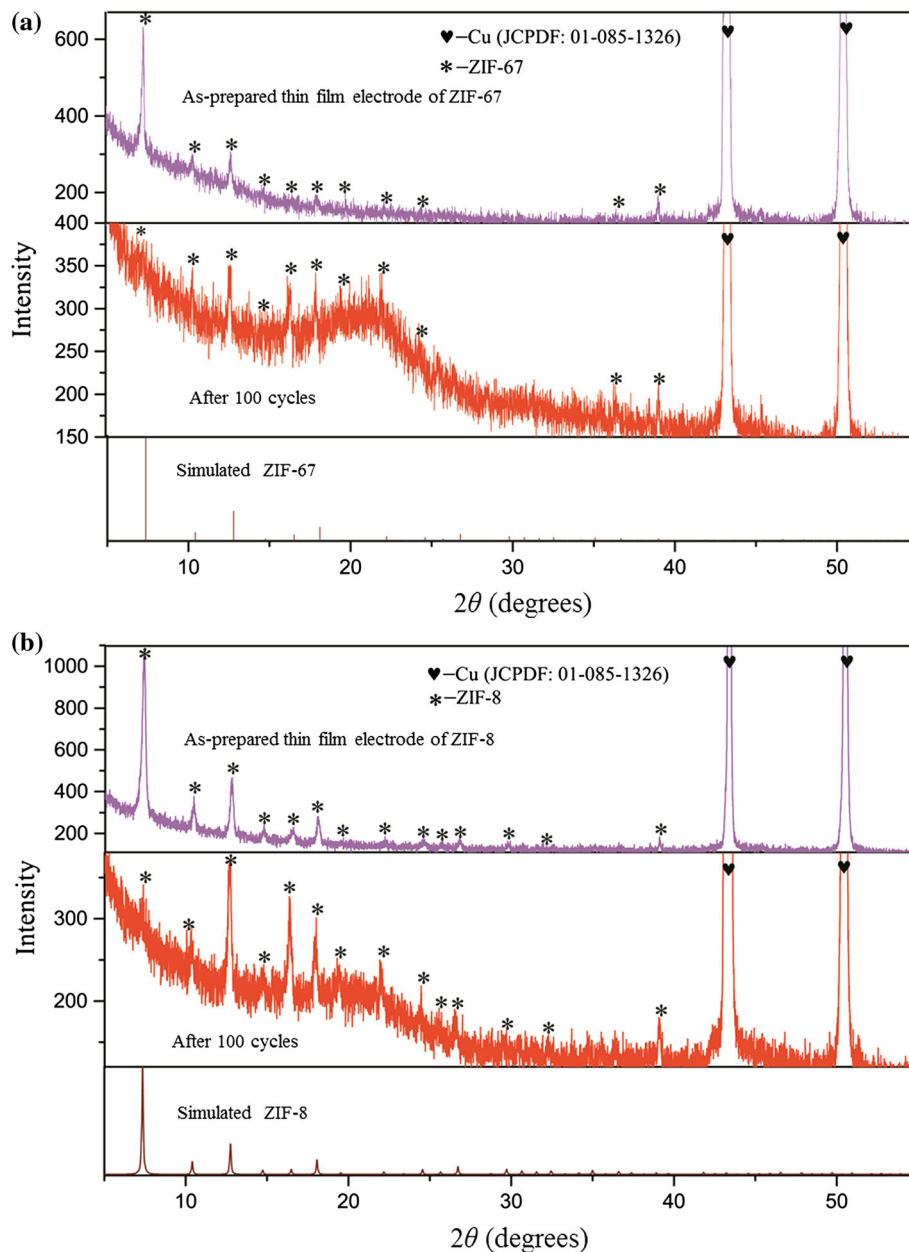
Two kinds of ZIFs, Zn-based ZIF-8 and Co-based ZIF-67, were prepared in this work following a facile synthetic method described in previous literatures [21, 22]. All the reagents, purchased from Shanghai Chemical Company, are of analytical grade and are used without any further purification.

The ZIF-8 and ZIF-67 film electrodes were prepared as follows: ZIF-8 and ZIF-67 slurries, each with a concentration of 3 mg mL<sup>-1</sup>, were obtained by treating a mixture of the ZIF and methanol in an ultrasonic bath at room temperature for 4 h. For the preparation of film electrodes, 0.2 mL of the sonicated suspension containing ZIF and methanol was directly drop cast onto a Cu foil current collector (1.5 cm<sup>2</sup>) and dried at 50 °C for half an hour under vacuum. Then the film electrodes were cooled down to room temperature.

### Characterization

The N<sub>2</sub> adsorption–desorption isotherms were measured on a Micromeritics ASAP 2460 analyzer. The samples were degassed in N<sub>2</sub> at 200 °C for 16 h prior to the measurements. The specific surface area was calculated with the Brunauer–Emmett–Teller (BET) equation, and the pore size distributions were calculated from the adsorption curve by the Barrett–Joyner–Halenda (BJH) method. The as-obtained film electrodes at different cycling states were analyzed by X-ray powder diffraction (XRD, Bruker D2 Phaser X-Ray Diffractometer) at a scan rate of 1° min<sup>-1</sup> with Cu-K $\alpha$  radiation. The microstructure and morphology of the fabricated film electrodes were investigated by scanning electron microscopy (SEM) on a JEOL-6700 microscope operating at 5 kV. Electrochemical tests of the prepared film electrodes were carried out using LIR2032 coin-type half cells that were assembled in a glove box with high-purity

**Figure 1** XRD patterns of ZIF-67 **a** and ZIF-8 **b** thin-film electrodes at different cycling states.



argon. The electrolyte was 1 M LiPF<sub>6</sub> in a 1:1 mixture (volume ratio) of ethylene carbonate (EC) and dimethyl carbonate (DMC). The counter electrode was a pure lithium foil. The charging and discharging curves were collected at different current densities within the range of 0.01–3.0 V on a battery testing system (NEWARE CT-3008). Electrochemical impedance spectroscopy (EIS) measurements were carried out on an electrochemical workstation (Shanghai Chen Hua CHI660D) to analyze the charge transfer processes using a sinusoidal signal of 5 mV within the frequency

range of 0.01 Hz–100 kHz. The impedance spectra were fitted using the iterating routine of the Zsimpwin software. The mass of loaded active material was measured using a microelectronic balance with an accuracy of 1 μg (Mettler Toledo XP6).

In order to see the morphological and molecular changes, the cells were disassembled in the glove box after cycling test and the electrodes were retrieved and then carefully washed with DMC and tetrahydrofuran for five and three times, respectively. After vacuum drying at 70 °C for 6 h, SEM and Fourier

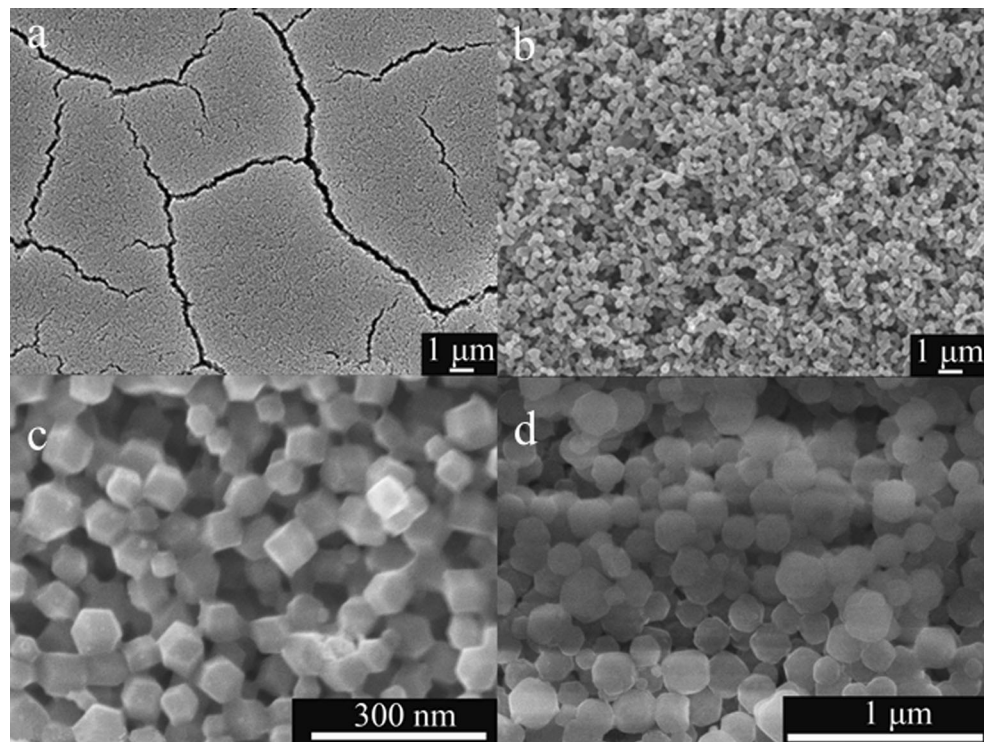


**Figure 2** SEM micrographs of a ZIF-8 thin-film electrode a, c and a ZIF-67 thin-film electrode b, d at different magnifications.

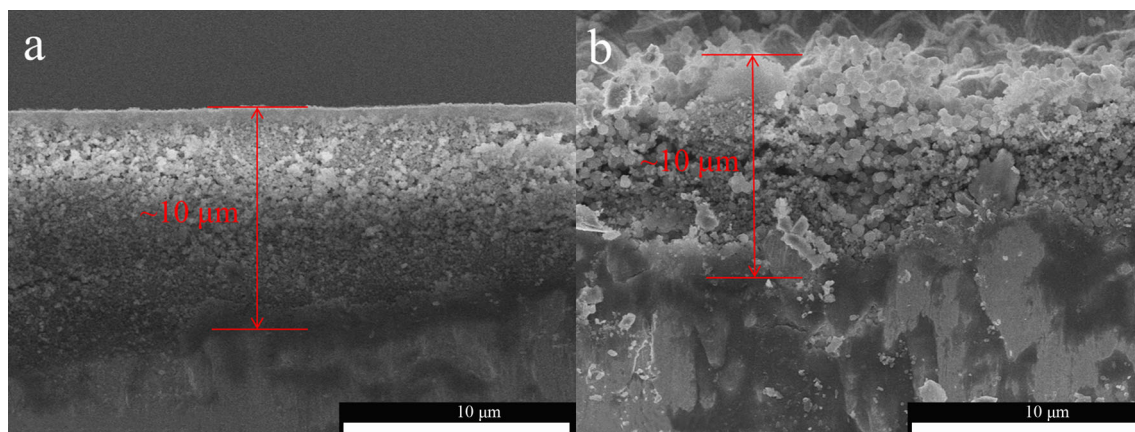


**Figure 3** The cross-sectional views of the as-prepared thin-film electrodes of ZIF-8 (a) and ZIF-67 (b).

transform infrared (FTIR) measurements were carried out.

## Results and discussion

Figure 1a, b shows the X-ray diffraction patterns of film electrodes prepared by the one-step strategy. As can be seen, all the as-prepared electrodes show well-defined diffraction peaks that are in good agreement

with the simulated patterns from the single crystal data of ZIF-67 and ZIF-8. The cubic Cu pattern (JCPDF: 01-085-1326) originates from the Cu foil that was used as a current collector. These results confirmed that the MOF materials had been pasted on Cu foil successfully. To obtain information on the microstructure and morphology of the film electrodes and on the thickness of the as-obtained film, SEM characterization on the as-prepared electrodes at different magnifications was carried out.

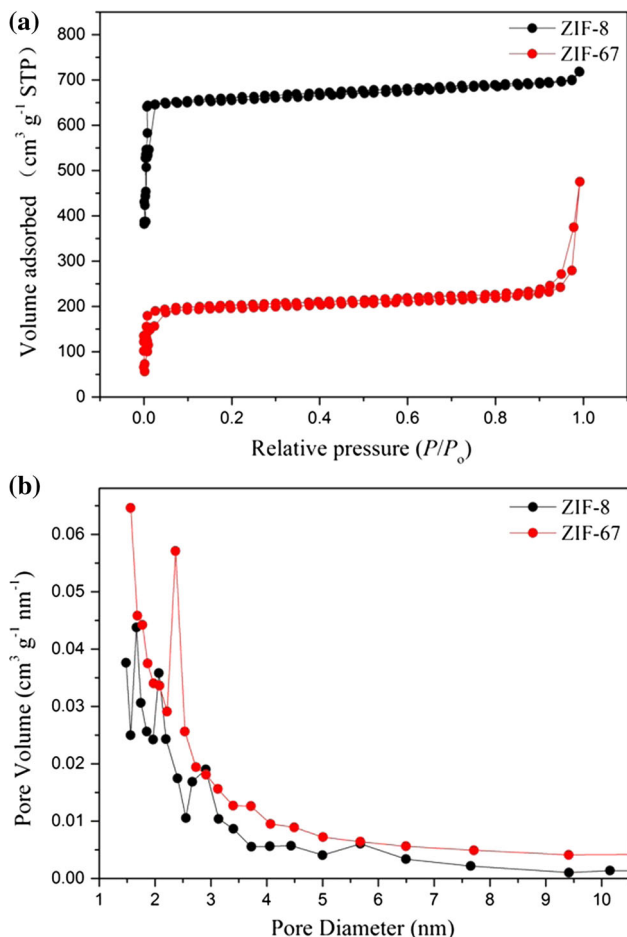


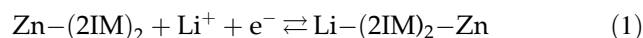
**Figure 4** a  $N_2$  adsorption–desorption isotherms of the as-prepared ZIF-8 and ZIF-67. b The corresponding pore size distributions calculated from the adsorption curve by the BJH method.

The SEM images of the thin-film electrodes show a uniform distribution of the MOF nanoparticles on the Cu substrate, with a few irregular cracks at intervals on the order of  $10\ \mu\text{m}$  (Fig. 2a, b). The high-resolution images (Fig. 2c, d) reveal a difference in average particle size for the two MOFs ( $\sim 50\ \text{nm}$  for ZIF-8,  $80\text{--}380\ \text{nm}$  for ZIF-67) [21, 22] and interstitial space between the nanoparticles. The thickness of the as-prepared film is about  $10\ \mu\text{m}$  (as shown in Fig. 3a, b). This porous thin-layer film structure is an intriguing feature, which ensures the effective permeation of the electrolytes during the charge and discharge processes. In addition, the cracks on the surface of film electrodes resulting from solvent evaporation during the heat treatment process can also serve as an accessible diffusion path for electrolyte species [23].

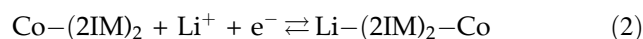
Nitrogen adsorption–desorption isotherms and pore size distribution graphs of the samples are

shown in Fig. 4. The ZIF-8 and ZIF-67 exhibit the similar hysteresis loops, implying the similar porosity for the two samples (as shown in Fig. 4b). The typical type I isotherms are indicative of adsorption in micropores due to strong adsorbent–adsorbate interactions [24]. A combination of mesopores with narrow size distribution center around 2.5 and 3 nm for ZIF-67 and ZIF-8, respectively, has been observed, indicating coexistence of structural pores as well as interparticle pores. The BET surface areas of ZIF-67 and ZIF-8 nanocrystals are calculated to be  $621$  and  $1858\ \text{m}^2\ \text{g}^{-1}$ , respectively, which are comparable with previous reports [21, 25]. The high surface area and porous host architectures can provide more active sites and allow rapid insertion of species, which are regarded as attractive features for lithium-ion electrode materials. However, the high surface area and predominant micropores might also lead to some side reactions such as reductive decomposition of the electrolyte and formation of a solid electrolyte interface (SEI) layer, resulting in the large initial irreversible capacity loss (ICL) and lower coulombic efficiency (CE).

Based on previous reports, we propose that Li ions may be stored within the pores of the MOFs because the Li ions have a strong interaction with N atoms in 2-methylimidazole (2IM) without the decomposition of the MOF structure during the charge and discharge processes [11], which is different from the mechanism for formate-bridged MOF ( $\text{Zn}_3(\text{HCOO})_6$ ) whose structure decomposes to form Zn nanoparticles [10]. The following reaction occurs in ZIF-8 film electrodes in assembled half cells:



which is equivalent to one mole of Li per formula unit. Similar electrochemical behavior has been reported for 3D  $\text{Zn}(\text{IM})_{1.5}(\text{abIM})_{0.5}$  and Mn-BTC MOFs electrodes [4, 11]. In addition, ZIF-67 is isostructural to ZIF-8 (the only difference is the transition-metal atom Co replacing the Zn atoms), which may also lead to similar electrochemical behavior during the discharge and charge processes [26]. In ZIF-67, the conversion reaction can be described as follows:



The X-ray diffraction patterns of the MOF thin-film electrodes after 100 cycles can also be used to further confirm the electrochemical behavior during the

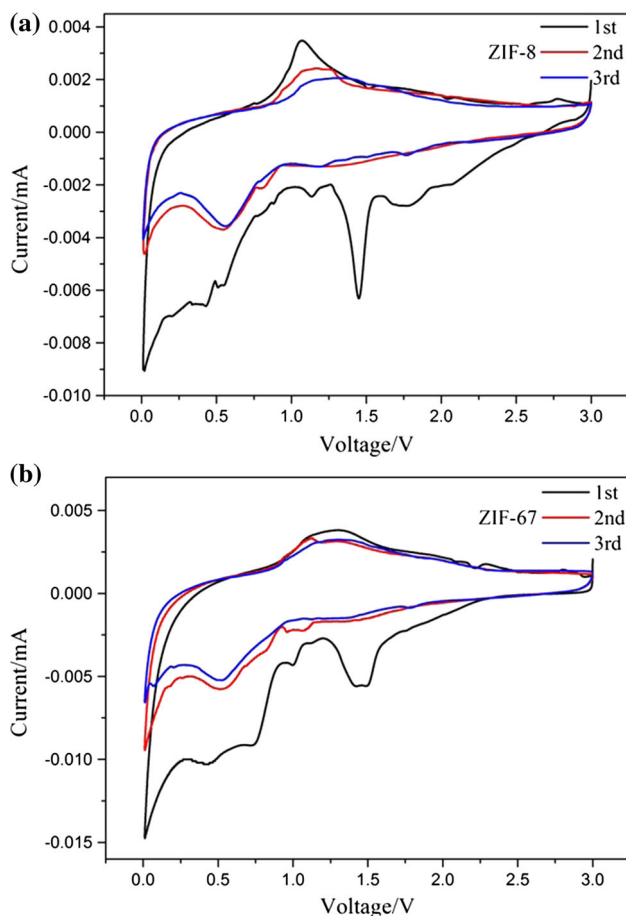


**Figure 5** Cyclic voltammograms of samples: **a** ZIF-8 and **b** ZIF-67.

charge and discharge processes (Fig. 1a, b). The presence of the characteristic MOF peaks indicates the high stability of the thin-film electrodes. Interestingly, no peaks other than the characteristic MOF peaks, such as Co and Zn, were detected for the cycled film electrodes, supporting the above hypothesis that the Li ions may react with the ligands of ZIFs and MOF structures will remain intact during the conversion reaction processes, which is similar to the previous reports [4, 11]. It is noteworthy that new broad peaks covering the range from  $20^\circ$  to  $26^\circ$  ( $2\theta$ ) have appeared in both XRD patterns after 100 cycles. This broad peak is more likely to be from a hydrocarbon  $(-\text{CH}_2\text{CH}_2-)_n$  polymer, which is a product of solvent decomposition and is present only at the SEI surface close to the electrolyte solution. According to the previous report, the major coproduct of EC reduction by ring opening is  $\text{CH}_2\text{CH}_2$ , which can either be liberated as ethylene gas, or polymerize on the electrode surface [27]. This could lead to a partial

polymerization and the formation of a hydrocarbon  $(-\text{CH}_2\text{CH}_2-)_n$  polymer [28]. Golodnitsky and co-workers found that the polymers content is as high as 30 at.% on the solution side of the SEI surface [29]. Therefore, the  $(-\text{CH}_2\text{CH}_2-)_n$  polymer can be detected in the Ex situ PXRD measurements. The XRD patterns of polyethylene provided in several previous reports demonstrate that the major broad peak of polyethylene is located at around  $24^\circ$  ( $2\theta$ ) [30, 31], which is in good agreement with the phenomenon observed in this study. However, the cycled film electrodes exhibited weaker diffraction peaks than the bare film electrodes, indicating that the crystallinity of the MOFs has decreased after cycling, which may be mainly attributed to the amorphization of active materials as a result of Li-ions insertion into the MOFs pores [10]. Li-ion insertion and de-intercalation results in the rearrangement of the MOF crystal structure in the electrolyte during the cycling tests [23]. On the basis of our above hypothesis (only one Li ion per formula unit), the theoretical capacities ( $C$ ) of ZIF-8 ( $\text{Zn}(\text{2IM})_2$ ) and ZIF-67 ( $\text{Co}(\text{2IM})_2$ ) can be calculated utilizing the following equation:

$$C = \frac{96500n}{3.6M}, \quad (3)$$

where  $n$  is the number of Li ions that were involved into the complete reaction ( $n = 1$ ) and  $M$  is the relative molecular mass of MOFs ( $M = 229.6$  and  $223.1 \text{ g mol}^{-1}$  for ZIF-8 and ZIF-67, respectively). Theoretical capacities for ZIF-8 and ZIF-67 were calculated to be 116.7 and 120  $\text{mAh g}^{-1}$ , respectively.

In order to further identify the redox processes of the film electrodes, cyclic voltammetry (CV) in the potential window of 0.01 to 3.0 V (vs.  $\text{Li}/\text{Li}^+$ ) was carried out and the initial three CV scans of ZIF-8 film electrodes are shown in Fig. 5a. During the first cathodic sweep for ZIF-8 anodes, two Li-insertion peaks occurred at about 1.8 and 1.5 V, respectively, and disappeared in the subsequent two cycles. These potential values are comparable to expected potential range for the amorphization of MOFs and the formation of Zn nanoparticles [10]. The broad reduction peak range from 0.6 to 0.01 V is probably corresponding to the formation of Li–Zn alloy [10]. In the successive first anodic sweep, there is a broad peak at about 1.2 V, and no oxidation peaks in the potential range of 0.01–0.85 V corresponding to the dealloying process of Li–Zn alloy can be observed. The absence of the dealloying peaks supports our above

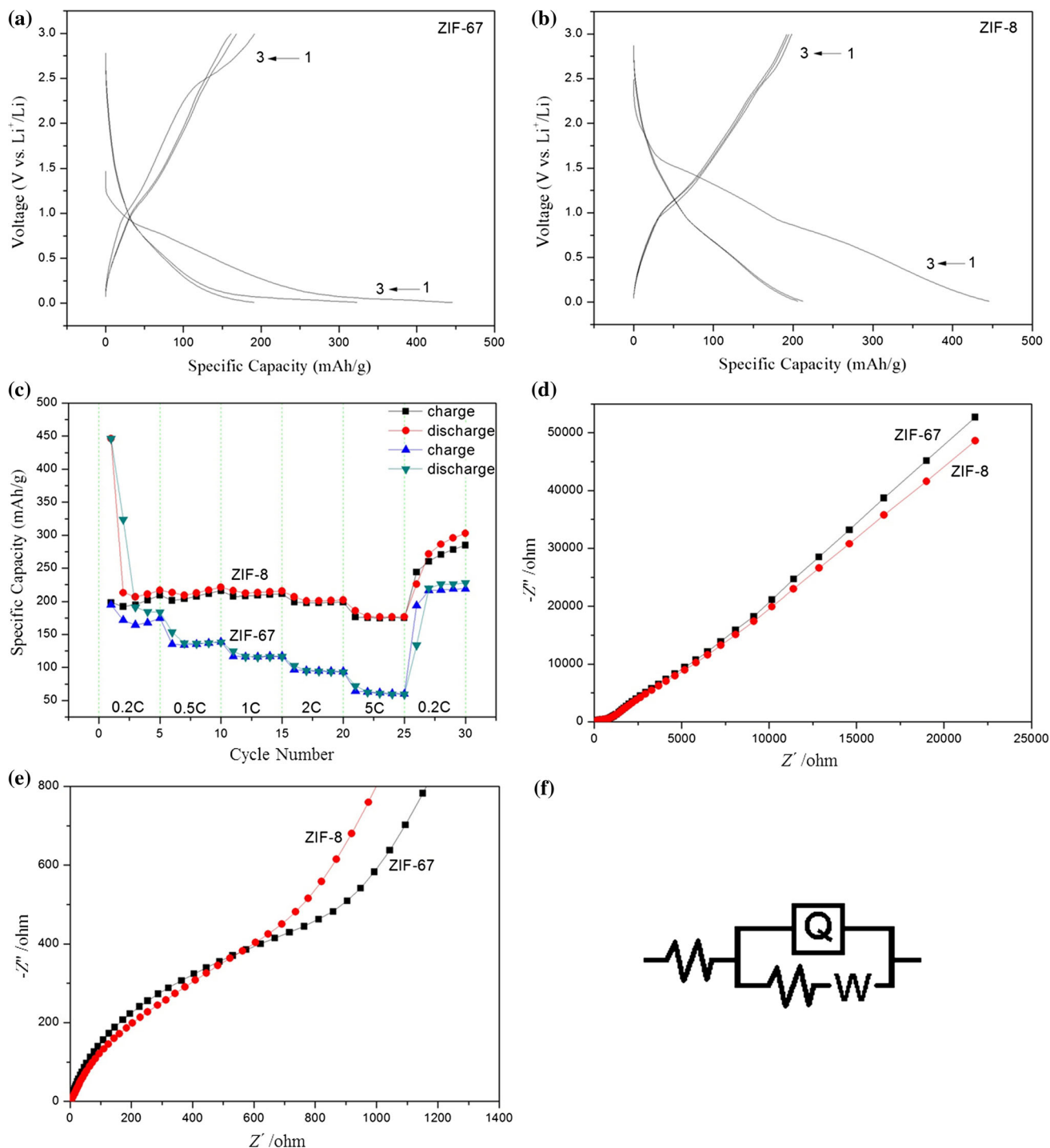


**Figure 6** Discharge/charge profiles of ZIF-67 (a) and ZIF-8 (b) thin-film electrodes at a current density of 0.2 C. c Rate performance test with increasing rate from 0.2 to 5 C with five cycles for each step. d Electrochemical impedance spectra of ZIF-

67 and ZIF-8 thin-film electrodes. e A magnified view of the Nyquist curves. f Corresponding equivalent circuit diagram for impedance spectra.

hypothesis that Li<sup>+</sup> ions may react with the ligands of the ZIF network without decomposing of MOFs structure and the formation of Zn particles, which is

different from the reported Zn<sub>3</sub>(HCOO)<sub>6</sub> electrodes [10]. A similar electrochemical behavior has been observed in 3D Zn(IM)<sub>1.5</sub>(abIM)<sub>0.5</sub> and Mn-BTC

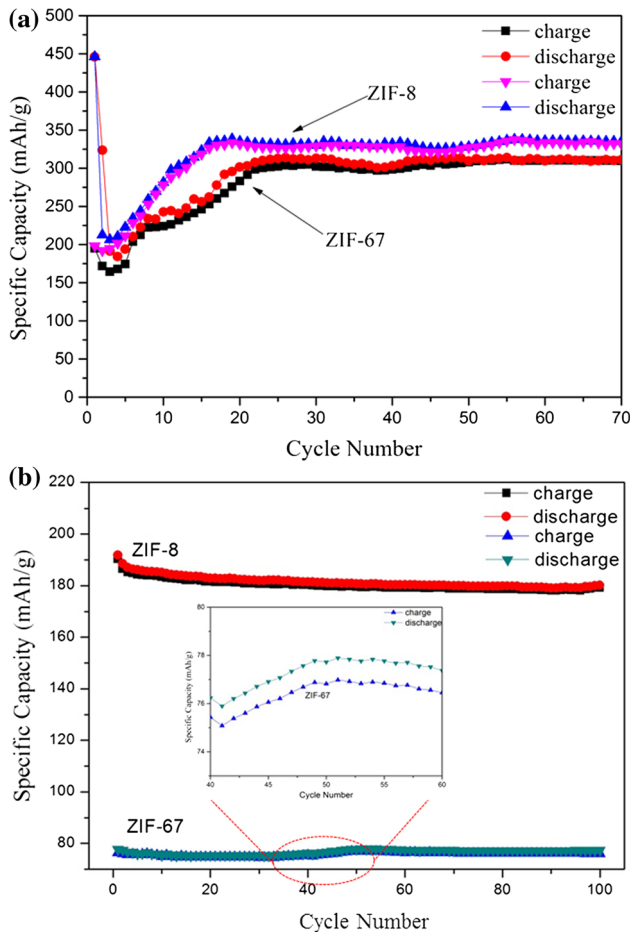


**Figure 7** Cycling tests of ZIF-67 and ZIF-8 thin-film electrodes at different current rates of 0.2C (a) and 5C (b).

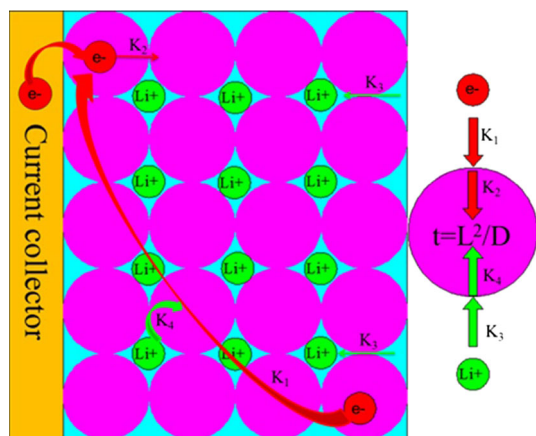
MOFs electrodes [4, 11]. From the second cycle onwards, it is noteworthy that the CV curves show a very good reproducibility without dramatically alteration in peak shape. Such an excellent replication of the CV curves demonstrates a good reversibility of  $\text{Li}^+$  ions extraction and insertion.

The initial three CV curves of ZIF-67 film electrodes are also presented in Fig. 5. It is easy to find that a similar conversion reaction with ZIF-8 film electrodes may possibly occur in ZIF-67 film anodes because of the extremely similar CV curves shape. Furthermore, as discussed previously, ZIF-67 is isostructural to ZIF-8, the only difference is the transition-metal atom replacing the Zn atoms with Co, which may also lead to the similar electrochemical behavior during the discharge and charge processes [26]. It is worth mentioning that the obvious long tail at potential below 0.6 V and broadening up to 0.01 V is also observed in the CV curves of ZIF-67 anodes as well as

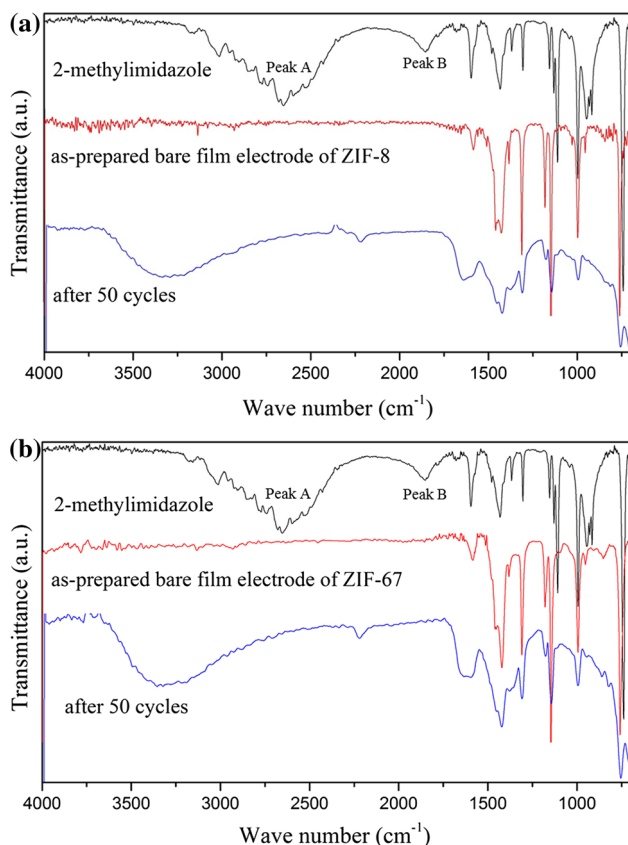
other MOF-based anodes [10, 32]. It is well accepted that metal Co does not alloy with Li, which suggest that the usual conversion mechanism might not be applicable to explain the Li storage in Zn-imidazole and Co-imidazole MOF. More importantly, XRD analysis, FTIR spectroscopy and SEM characterization of the ZIF electrodes at the different cycling states failed to indicate decomposition of ZIFs and presence of Zn and Co (FTIR and SEM characterization will be discussed later). These observations lead us to the conclusion that lithiation likely occurs at the 2-methylimidazole ligands rather than at central metal ions, resulting in a distortion of the ZIFs network. A similar conclusion has been proposed in some previous literatures [4, 32]. Moreover, the very broad nature of the redox peaks is probably indicative of gradual multistep Li-insertion process [4].

Figure 6a, b shows the charge and discharge voltage profiles of ZIF-67 and ZIF-8 thin-film electrodes for the initial three cycles at a current density of 0.2 C. For ZIF-67/Li half cells, the first discharge and charge capacities are as high as 446.1 and 191.7  $\text{mAh g}^{-1}$ , respectively, with a CE of 43%. During the second cycle, the discharge capacity has decreased to 323.5  $\text{mAh g}^{-1}$ , indicating that about 27.5% of the initial discharge capacity is irreversible, which may be related to the formation of SEI layer and the decomposition of the electrolyte after the first cycle [10]. The third cycle discharge capacity was only 189.9  $\text{mAh g}^{-1}$ , corresponding to the second discharge capacity fading of 41%. Compared to the ZIF-67/Li half cells, the ZIF-8 film electrodes delivered a discharge capacity of 446.1 and 212.8  $\text{mAh g}^{-1}$  in the initial two cycles with 52.3% ICL, which is a little higher than the ZIF-67 anode. The second and third discharge capacities for the ZIF-8 thin-film electrode were 212.8, and 206.5  $\text{mAh g}^{-1}$ , respectively, demonstrating that it had a smaller ICL (about 3%) after the first discharge process. From the first cycle onwards, the ZIF-8 thin-film electrode shows a very good replication of the voltage–capacity contour, demonstrating a good reversibility of Li ion extraction and insertion. However, large initial capacity losses are noted for ZIF-67 and ZIF-8, which are mainly due to the electrolyte decomposition [33]. Some saturated solvent molecules within the ZIFs pores may also have contributed to this irreversible capacity [10]. The fact that observed capacities were higher than the theoretical capacities suggests that more than one Li is accommodated per formula unit,





**Scheme 1** Schematic illustration of the transfer and diffusion processes of both electrons and lithium ions in thin-film electrodes.  $K_1$  to  $K_4$  refer to charge transfer kinetics (electrode surface), charge diffusion kinetics (crystal lattice), Li-ion diffusion kinetics (electrolyte), and Li-ion diffusion kinetics (crystal lattice), respectively.



**Figure 8** FTIR spectra of the as-prepared ZIF-8 (a) and ZIF-67 (b) film electrodes at different cycling states.

in contrast to our original hypothesis. The determination of the additional Li storage sites in these MOFs will require further study.

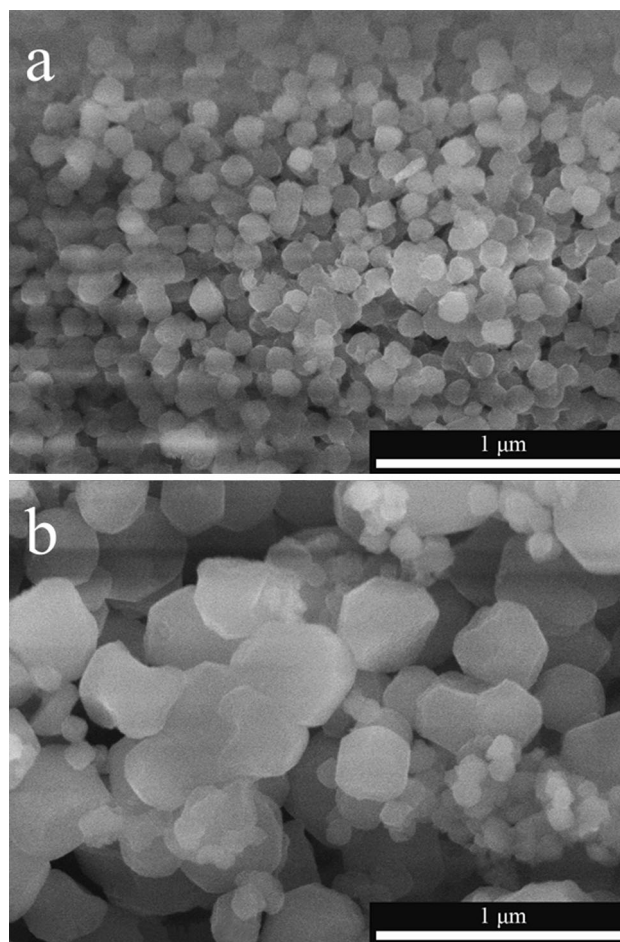


**Figure 9** SEM images of the ZIF-8 (a) and ZIF-67 (b) film electrodes after 50 cycles at a current density of 5 C.

The rate test performance data of ZIF-8 and ZIF-67 thin-film electrodes are presented in Fig. 6c. The average discharge capacities of ZIF-8 electrodes for each five cycles at 0.2, 0.5, 1, 2, and 5 C were 258.2, 214.2, 214.0, 202.0, and 178.2 mAh g<sup>-1</sup>, respectively. When the current density was decreased back to 0.2 C, the discharge capacity even increased up to 280 mAh g<sup>-1</sup>, which is slightly higher than the initial average discharge capacity. This phenomenon has also been observed in ZIF-67 film electrode and 3D Zn(IM)<sub>1.5</sub>(abIM)<sub>0.5</sub> electrodes [11]. For ZIF-67 thin-film electrodes, the average discharge capacities were calculated to be 265, 139, 118, 96, and 63 mAh g<sup>-1</sup> at 0.2, 0.5, 1, 2, and 5 C, respectively. It can be found that ZIF-8 thin-film electrodes exhibit a higher rate performance than that of ZIF-67 thin-film electrodes, which might be attributed to the smaller particle size of ZIF-8 [21, 22]. The smaller particle size can shorten diffusion path of Li ions, resulting in the good rate

performance (as shown in graphic abstract). In order to further confirm the charge transfer behavior, EIS tests were also carried out (as shown in Fig. 6d, e). Each of Nyquist plots is composed of an approximately 45° inclined line in the low-frequency range (as shown in Fig. 6d), which could be considered as Warburg impedance ( $Z_W$ ), corresponding the lithium-ion diffusion in the bulk of the active material and a compressed semicircle in the high- to medium-frequency range, which describe the charge transfer resistance ( $R_{ct}$ ) for these electrodes (as shown in Fig. 6e). The impedance data were analyzed by the fitting to an equivalent electrical circuit shown in Fig. 6f, similar to the circuit employed for other MOF-based anodes [4]. After simulating the compressed semicircle for both samples, the value of  $R_{ct}$  for the ZIF-8 electrode was calculated to be 611.9  $\Omega$ , while the value of  $R_{ct}$  for the ZIF-67 anode was calculated to be 680.5  $\Omega$ . The ZIF-8 thin-film electrode showed a relatively lower charge transfer resistance ( $R_{ct}$ ) than the ZIF-67 thin-film electrode, which is in agreement with the above analysis that is, smaller particle size will shorten the diffusion length.

Figure 7a presents their long-cycle characteristics up to 70 cycles at a current rate of 0.2 C. For the ZIF-8 film anode, the discharge capacity decreases to a minimum value of 210.6 mAh g<sup>-1</sup> over the initial five cycles, then it increases gradually to 338.5 mAh g<sup>-1</sup> during the subsequent ten cycles, and finally it delivers an almost stable discharge capacity of about 335.3 mAh g<sup>-1</sup> from the 15th to the 70th cycle. A similar phenomenon has also been observed in the ZIF-67 film anode, which delivers an almost constant discharge capacity of about 311.6 mAh g<sup>-1</sup> after the first 20 cycles. The increasing trend of discharge capacity from the 5th to 20th cycle has been widely observed in the previous reports, which can be assigned to the reversible growth of a polymeric gel-like film on the surface of the active materials [3, 34, 35]. Meanwhile, the equilibration and activation of the electrode in the first 20 cycles should also be responsible to this capacity rise phenomenon [4]. The wetting of the electrode surface by the electrolyte may increase with extensive cycling as has been observed for both MOFs [4, 36] and other materials [37]. The cycling stability of the thin-film electrodes was further evaluated at a high current density of 5 C for 100 cycles (Fig. 7b). The initial and 100th discharge capacities for ZIF-8 film

electrode were 188.6 and 179.2 mAh g<sup>-1</sup>, respectively (about 4.5% initial capacity loss). Such an excellent cycling stability can be mainly attributed to the following two reasons. Firstly, MOFs were directly drop cast onto Cu foils without any binder and conductive additives, which can improve volumetric utilization efficiency and increase surface area of the electrode [38]. The enlarged surface area ensures locally lower current densities and creates more surface sites for lithium to enter the electrode material [39]. Secondly, Li ions can be stored within the MOFs pores without the collapse of MOFs structure, leading to an exceptional reversibility [11]. These merits combined with the synergistic effect of smaller particle size may be responsible for the good electrochemical performance. Unlike the ZIF-8 film electrodes, the initial and 100th discharge capacities for ZIF-67 film electrode were much lower (78.3 and 77.5 mAh g<sup>-1</sup>, respectively). More importantly, there is an obvious fluctuation around the 40th cycle for the ZIF-67 film electrode and the discharge capacity gradually increased from 75.9 to 77.9 mAh g<sup>-1</sup>. This fluctuation is in good agreement with the above analysis, that is, the relatively larger particle size may prolong the period of time required for Li ions to penetrate the entire electrode materials.

Ex situ FTIR measurements of the film electrodes at different cycling states were also carried out. As shown in Fig. 8, significant differences are observed in the spectrum of 2-methylimidazole and bare film electrodes. The broad and strong absorption peaks due to vibrations of the hydrogen bonds established between the pyrrole group and the pyridinic nitrogen (N–H...N) in the range of 2200–3200 cm<sup>-1</sup> (Peak A) completely disappeared in the two bare film electrodes, which matched well with the previous report [40], suggesting that central metal ions (Co<sup>2+</sup> and Zn<sup>2+</sup>) have been coordinated with the 2-methylimidazole ligands successfully. The absorption peak emerged at about 1844 cm<sup>-1</sup> (Peak B) can be ascribed to the resonance between the N–H...N bending “out of plane” and the N–H stretching vibrations, which also cannot be detected in the spectrum of the bare film electrodes, further indicating the formation of the ZIF structure [41]. After cycling test, the presence of the peaks associated with the coordinated 2-methylimidazole in the FTIR spectrum of both cycled film electrodes demonstrates the structural sustenance of the ZIF network.

Morphological changes of the cycled film anodes were characterized by SEM measurements. The SEM images of the two cycled film electrodes in Fig. 9a, b inform that the ZIF particles did not suffer severe morphological changes due to the conversion reaction.

As illustrated in Scheme 1, eliminating the need of binder is favorable for transport of electrons between ZIF particles and the current collector [42]. The thin-layer architecture can ensure a fast  $\text{Li}^+$  diffusion through the whole electrode, because of the shortened diffusion paths. The experimental results demonstrate that the thin-film electrodes have a high specific capacity (specific capacities for ZIF-8 and ZIF-67 are 335.3 and 311.6  $\text{mAh g}^{-1}$ , respectively, at a current density of 0.2 C) and exceptional cycling stability (about 95.5% initial capacity loss was retained after 100 cycles at a high current density of 5 C). Such an outstanding performance and simple fabrication method may provide a feasible approach for LIBs applications.

## Conclusions

In summary, MOF thin-film electrodes with a uniform thin-layer structure were successfully prepared by a drop-casting method using MOF slurries. Such a simple conductive agent- and binder-free route greatly simplifies the conventional preparation method with the need for PVDF (polymer binder) and Super P (conductive carbon black), and provides a new possible solution for the preparation of electrodes. Although the electrodes exhibited a large ICL after the first discharge process, the reversible capacities were still as high as 335.3 and 311.6  $\text{mAh g}^{-1}$  for ZIF-8 and ZIF-67, respectively. More interestingly, these film electrodes delivered an exceptionally cycling stability (only 4.5% initial capacity loss after 100 cycles at a high current density of 5 C) and a good rate performance.

## Acknowledgements

This project is sponsored by the Shanghai University of Engineering Science Innovation Fund for Graduate Students (16KY0404) and the National Natural Science Foundation of China (11602134), and supported by the Shanghai Municipal Education Commission (High-energy Beam Intelligent Processing and Green

Manufacturing) and the University of Minnesota Initiative for Renewable Energy and the Environment (IREE). Parts of this work were carried out in the Characterization Facility, University of Minnesota, which receives partial support from the NSF through the MRSEC program.

## References

- [1] Xu X, Cao R, Jeong S, Cho J (2012) Spindle-like mesoporous  $\alpha\text{-Fe}_2\text{O}_3$  anode material prepared from MOF template for high-rate lithium batteries. *Nano Lett* 12:4988–4991. doi:10.1021/nl302618s
- [2] Yim C-H, Baranova EA, Courtel FM, Abu-Lebdeh Y, Davidson IJ (2011) Synthesis and characterization of macroporous tin oxide composite as an anode material for Li-ion batteries. *J Power Sources* 196:9731–9736. doi:10.1016/j.jpowsour.2011.07.061
- [3] Liu X, Zhao J, Hao J, Su B-L, Li Y (2013) 3D ordered macroporous germanium fabricated by electrodeposition from an ionic liquid and its lithium storage properties. *J Mater Chem A* 1:15076–15081. doi:10.1039/c3ta12923c
- [4] Maiti S, Pramanik A, Manju U, Mahanty S (2015) Reversible lithium storage in manganese 1,3,5-benzenetricarboxylate metal-organic framework with high capacity and rate performance. *ACS Appl Mater Interfaces* 7:16357–16363. doi:10.1021/acsami.5b03414
- [5] Furukawa H, Cordova KE, O’Keeffe M, Yaghi OM (2013) The chemistry and applications of metal-organic frameworks. *Science* 341:1230444–1230456. doi:10.1126/science.1230444
- [6] Gao Y, Wu J, Zhang W, Tan Y, Gao J, Tang B, Zhao J (2015) Synthesis of nickel carbonate hydroxide@zeolitic imidazolate framework-67 ( $\text{Ni}_2\text{CO}_3(\text{OH})_2@ZIF-67$ ) for pseudocapacitor applications. *J Appl Electrochem* 45:541–547. doi:10.1007/s10800-015-0795-2
- [7] Han Y, Qi P, Li S, Feng X, Zhou J, Li H, Su S, Li X, Wang B (2014) A novel anode material derived from organic-coated ZIF-8 nanocomposites with high performance in lithium ion batteries. *Chem Commun* 50:8057–8060. doi:10.1039/c4cc02691h
- [8] Han X, Yi F, Sun T, Sun J (2012) Synthesis and electrochemical performance of Li and Ni 1,4,5,8-naphthalenetetracarboxylates as anodes for Li-ion batteries. *Electrochem Commun* 25:136–139. doi:10.1016/j.elecom.2012.09.014
- [9] Férey G, Millange F, Morcrette M, Serre C, Doublet M-L, Grenèche J-M, Tarascon J-M (2007) Mixed-valence Li/Fe-based metal-organic frameworks with both reversible redox and sorption properties. *Angew Chem Int Edit* 46:3259–3263. doi:10.1002/anie.200605163

- [10] Saravanan K, Nagarathinam M, Balaya P, Vittal JJ (2010) Lithium storage in a metal organic framework with diamondoid topology—a case study on metal formates. *J Mater Chem* 20:8329–8335. doi:10.1039/c0jm01671c
- [11] Lin YZ, Zhang Q, Zhao C, Li H, Kong C, Shen C, Chen L (2015) An exceptionally stable functionalized metal-organic framework for lithium storage. *Chem Commun* 51:697–699. doi:10.1039/c0xx00000x
- [12] Zhao Y, Song Z, Li X, Sun Q, Cheng N, Lawes S, Sun X (2016) Metal organic frameworks for energy storage and conversion. *Energy Storage Mater* 2:35–62. doi:10.1016/j.ensm.2015.11.005
- [13] Ameloot R, Aubrey M, Wiers BM, Gomora-Figueroa AP, Patel SN, Balsara NP, Long JR (2013) Ionic conductivity in the metal–organic framework UiO-66 by dehydration and insertion of lithium tert-butoxide. *Chem-Eur J* 19:5533–5536. doi:10.1002/chem.201300326
- [14] Gao Y, Wu J, Zhang W, Tan Y, Gao J, Zhao J, Tang B (2014) The calcined zeolitic imidazolate framework-8 (ZIF-8) under different conditions as electrode for supercapacitor applications. *J Solid State Electrochem* 18:3203–3207. doi:10.1007/s10008-014-2578-9
- [15] Worrall SD, Mann H, Rogers A, Bissett MA, Attfield MP, Dryfe RAW (2016) Electrochemical deposition of zeolitic imidazolate framework electrode coatings for supercapacitor electrodes. *Electrochim Acta* 197:228–240. doi:10.1016/j.electacta.2016.02.145
- [16] Zhang G, Hou S, Zhang H, Zeng W, Yan F, Li CC, Duan H (2015) High-performance and ultra-stable lithium-ion batteries based on MOF-derived ZnO@ZnO quantum dots/C core-shell nanorod arrays on a carbon cloth anode. *Adv Mater* 27:2400–2405. doi:10.1002/adma.201405222
- [17] Wang N, Wu C, Li J, Dong G, Guan L (2011) Binder-free manganese oxide/carbon nanomaterials thin film electrode for supercapacitors. *ACS Appl Mater Interfaces* 3:4185–4189. doi:10.1021/am201145k
- [18] Tian B, Światowska J, Maurice V, Zanna S, Seyeux A, Klein LH, Marcus P (2013) Combined surface and electrochemical study of the lithiation/delithiation mechanism of the iron oxide thin-film anode for lithium-ion batteries. *J Phys Chem C* 117:21651–21661. doi:10.1021/jp4064438
- [19] Stassen I, Styles M, Van Assche T, Campagnol N, Fransaeer J, Denayer J, Tan J-C, Falcaro P, De Vos D, Ameloot R (2015) Electrochemical film deposition of the zirconium metal–organic framework UiO-66 and application in a miniaturized sorbent trap. *Chem Mater* 27:1801–1807. doi:10.1021/cm504806p
- [20] Yiping T, Xiaoxu T, Guangya H, Guoqu Z (2014) Nanocrystalline Li<sub>4</sub>Ti<sub>5</sub>O<sub>12</sub>-coated TiO<sub>2</sub> nanotube arrays as three-dimensional anode for lithium-ion batteries. *Electrochim Acta* 117:172–178. doi:10.1016/j.electacta.2013.11.095
- [21] Qian J, Sun F, Qin L (2012) Hydrothermal synthesis of zeolitic imidazolate framework-67 (ZIF-67) nanocrystals. *Mater Lett* 82:220–223. doi:10.1016/j.matlet.2012.05.077
- [22] Torad NL, Hu M, Kamachi Y, Takai K, Imura M, Naito M, Yamauchi Y (2013) Facile synthesis of nanoporous carbons with controlled particle sizes by direct carbonization of monodispersed ZIF-8 crystals. *Chem Commun* 49:2521–2523. doi:10.1039/c3cc38955c
- [23] Lee DY, Yoon SJ, Shrestha NK, Lee S-H, Ahn H, Han S-H (2012) Unusual energy storage and charge retention in Co-based metal–organic-frameworks. *Micropor Mesopor Mater* 153:163–165. doi:10.1016/j.micromeso.2011.12.040
- [24] Kruk M, Jaroniec M (2001) Gas adsorption characterization of ordered organic – inorganic nanocomposite materials. *Chem Mater* 13:3169–3183. doi:10.1021/cm0101069
- [25] Park KS, Ni Z, Cote AP, Choi JY, Huang R, Uribe-Romo FJ, Chae HK, O’Keeffe M, Yaghi OM (2006) Exceptional chemical and thermal stability of zeolitic imidazolate frameworks. *Proc Natl Acad Sci USA* 103:10186–10191. doi:10.1073/pnas.0602439103
- [26] Banerjee R, Phan A, Wang B, Knobler C, Furukawa H, O’Keeffe M, Yaghi OM (2008) High-throughput synthesis of zeolitic imidazolate frameworks and application to CO<sub>2</sub> capture. *Science* 319:939–943. doi:10.1126/science.1152516
- [27] Aurbach D, Markovsky B, Weissman I, Levi E, Ein-Eli Y (1999) On the correlation between surface chemistry and performance of graphite negative electrodes for Li ion batteries. *Electrochim Acta* 45:67–86. doi:10.1016/s0013-4686(99)00194-2
- [28] Eriksson T, Andersson AM, Bishop AG, Gejke C, Tr Gustafsson, Thomas JO (2002) Surface analysis of LiMn[<sub>sub</sub> 2]O[<sub>sub</sub> 4] electrodes in carbonate-based electrolytes. *J Electrochem Soc* 149(1):A69–A78. doi:10.1149/1.1426398
- [29] Eshkenazi V, Peled E, Burstein L, Golodnitsky D (2004) XPS analysis of the SEI formed on carbonaceous materials. *Solid State Ionics* 170:83–91. doi:10.1016/s0167-2738(03)00107-3
- [30] L-j Huang, B-j Li, N-f Ren (2016) Enhancing optical and electrical properties of Al-doped ZnO coated polyethylene terephthalate substrates by laser annealing using overlap rate controlling strategy. *Ceram Int* 42:7246–7252. doi:10.1016/j.ceramint.2016.01.118
- [31] Mannan TM, Soares JBP, Berry RM, Hamad WY (2016) In-situ production of polyethylene/cellulose nanocrystal composites. *Can J Chem Eng* 94:2107–2113. doi:10.1002/cjce.22608
- [32] Tang B, Huang S, Fang Y, Hu J, Malonzo C, Truhlar DG, Stein A (2016) Mechanism of electrochemical lithiation of a

- metal-organic framework without redox-active nodes. *J Chem Phys* 144:194702–194705. doi:[10.1063/1.4948706](https://doi.org/10.1063/1.4948706)
- [33] Liu Q, Yu L, Wang Y, Ji Y, Horvat J, Cheng ML, Jia X, Wang G (2013) Manganese-based layered coordination polymer: synthesis, structural characterization, magnetic property, and electrochemical performance in lithium-ion batteries. *Inorg Chem* 52:2817–2822. doi:[10.1021/ic301579g](https://doi.org/10.1021/ic301579g)
- [34] Liu Y, Bai J, Ma X, Li J, Xiong S (2014) Formation of quasi-mesocrystal  $ZnMn_2O_4$  twin microspheres via an oriented attachment for lithium-ion batteries. *J Mater Chem A* 2:14236–14244. doi:[10.1039/c4ta02950j](https://doi.org/10.1039/c4ta02950j)
- [35] Cherian CT, Sundaramurthy J, Reddy MV, Suresh Kumar P, Mani K, Pliszka D, Sow CH, Ramakrishna S, Chowdari BV (2013) Morphologically robust  $NiFe_2O_4$  nanofibers as high capacity Li-ion battery anode material. *ACS Appl Mater Interfaces* 5:9957–9963. doi:[10.1021/am401779p](https://doi.org/10.1021/am401779p)
- [36] Worrall SD, Bissett MA, Hirunpinyopas W, Attfield MP, Dryfe RAW (2016) Facile fabrication of metal–organic framework HKUST-1-based rewritable data storage devices. *J Mater Chem C* 4:8687–8695. doi:[10.1039/c6tc03496a](https://doi.org/10.1039/c6tc03496a)
- [37] Bissett MA, Kinloch IA, Dryfe RA (2015) Characterization of  $MoS_2$ -graphene composites for high-performance coin cell supercapacitors. *ACS Appl Mater Interfaces* 7(31):17388–17398. doi:[10.1021/acsami.5b04672](https://doi.org/10.1021/acsami.5b04672)
- [38] Li Y, Trujillo MA, Fu E, Patterson B, Fei L, Xu Y, Deng S, Smirnov S, Luo H (2013) Bismuth oxide: a new lithium-ion battery anode. *J Mater Chem A* 1:12123–12127. doi:[10.1039/C3TA12655B](https://doi.org/10.1039/C3TA12655B)
- [39] Tonti D, MaJ Torralvo, Enciso E, Sobrados I, Sanz J (2008) Three-dimensionally ordered macroporous lithium manganese oxide for rechargeable lithium batteries. *Chem Mater* 20:4783–4790. doi:[10.1021/cm702134s](https://doi.org/10.1021/cm702134s)
- [40] Bustamante EL, Fernandez JL, Zamaro JM (2014) Influence of the solvent in the synthesis of zeolitic imidazolate framework-8 (ZIF-8) nanocrystals at room temperature. *J Colloid Interface Sci* 424:37–43. doi:[10.1016/j.jcis.2014.03.014](https://doi.org/10.1016/j.jcis.2014.03.014)
- [41] Li X, Gao X, Ai L, Jiang J (2015) Mechanistic insight into the interaction and adsorption of Cr(VI) with zeolitic imidazolate framework-67 microcrystals from aqueous solution. *Chem Eng J* 274:238–246. doi:[10.1016/j.cej.2015.03.127](https://doi.org/10.1016/j.cej.2015.03.127)
- [42] Polat DB, Lu J, Abouimrane A, Keles O, Amine K (2014) Nanocolumnar structured porous Cu-Sn thin film as anode material for lithium-ion batteries. *ACS Appl Mater Interfaces* 6:10877–10885. doi:[10.1021/am405994b](https://doi.org/10.1021/am405994b)